APPENDIX 2

D1-25
51P.

N87-16086

Calculated Potential Surfaces for the Reactions:

$$O + N_2 \rightarrow NO + N$$

and

$$N + O_2 \rightarrow NO + O$$

Stephen P. Walch[a]
Eloret Institute
Sunnyvale, CA 94087

and

Richard L. Jaffe
NASA Ames Research Center
Moffett Field, CA 94035

Abstract

Complete Active Space SCF/ Contracted CI (CASSCF/CCI) calculations, using large gaussian basis sets, are presented for selected portions of the potential surfaces for the reactions in the Zeldovich mechanism for the conversion of N_2 to NO. The N + O_2 reaction is exoergic by 32 kcal/mole and is computed to have an early barrier of 10.2 kcal/mole for the $^2A'$ surface and 18.0 kcal/mole for the $^4A'$ surface. The O + N_2 reaction is endoergic by 75 kcal/mole. The $^3A''$ surface is calculated to have a late barrier of 0.5 kcal/mole, while the $^3A'$ surface is calculated to have a late barrier of 14.4 kcal/mole.

[a]Mailing Address: NASA Ames Research Center, Moffett Field, CA 94035.

I. Introduction

Aeroassisted orbital transfer vehicles (AOTVs) will be designed to use the aerodynamic forces produced over the surface of a large heat shield (possibly 100 meters in diameter) to permit transfer between high and low altitude earth orbits with reduced use of rocket propulsion for manuvering. During these orbital transfer trajectories the vehicle will be subjected to substantial radiative and convective heat transfer from the bow shock wave to the heat shield. By operating at high altitudes ($>$ 70 km), where the atmospheric density is low, convective heating is reduced, but nonequilibrium radiation enhancement[1] is significant. The air in the shock layer which forms in front of the AOTV is at sufficiently low pressure that, while the rotational and translational modes of the molecules may be equilibrated, the vibrational and electronic degrees of freedom will definitely not be equilibrated. It is reasonable to characterize the various energy modes by different temperatures. Expected values of the translational and rotational temperatures here are in the range of 10000-50000K (about 1-5 eV), while the vibrational and electronic temperatures are typically less than 15000K. The physical and chemical phenomena occuring under these conditions are poorly understood, and existing laboratory data show uncertainties of a factor of about 4 for important rate constants at the flight velocities anticipated for the AOTV[2]. Attempts are currently being made to model these processes[2-3].

Among input needed to model the characteristics of such high temperature nonequilibrium air is a kinetic data base for several classes of air reactions. Among these are i) charge transfer processes such as $N + N^+ \rightarrow N^+ + N$ [4], dissociative processes such as $N_2 + N \rightarrow N + N + N$ [5], and the atomic molecular exchange processes studied in the present paper: $N + O_2 \rightarrow NO + O$, and $O + N_2 \rightarrow NO + N$. Since the electronic temperature may be greater than 10000K, excited state reactions may also be important. For example at 10000K 16.4 % of the O_2 molecules are in the $^1\Delta_g$ state and 5.4 % of the O atoms and 13.3 % of the N atoms are in the ^{1}D and ^{2}D states, respectively. The excited electronic state reactions $N(^2D) + O_2$ and $N + O_2(^1\Delta_g)$ are believed to be faster than the corresponding ground state reactions at low temperatures[6]. They occur on potential energy surfaces which directly connect to ground state products with little or no activation

barriers and are also highly exothermic. At high temperatures, however, the rate constants will be limited by the overall collision rate which should be nearly the same for each reaction. In the case of the N_2 + $O(^1D)$ reaction, the adiabatic potential energy surfaces lead to electronically excited products ($NO^2\Pi$ + $N(^2P)$) and contain a deep energy minimum corresponding to the stable N_2O molecular electronic ground state. It is not believed that this highly endothermic reaction will make a significant contribution to the rate constants even at extremely high temperatures.

As a start in understanding the kinetics and dynamics of these systems we have studied the ground state potential energy surfaces. These surfaces will be used to compute rate constants at high temperatures and for non-equilibrium conditions where experimental data are not available. The reactions studied here are also important at lower temperatures in hydrocarbon combustion as the Zeldovich mechanism for conversion of air N_2 to NO_x [7].

A semi-quantitative study of the potential energy surfaces for the N + O_2 → NO + O reaction has been carried out by Das and Benioff[8] using MCSCF and limited CI calculations. The current study includes more extensive electron correlation and uses a much more extensive basis set than in Ref. 8. The O + N_2 reaction has also been discussed by Jaffe [3] using a phenomenological collision theory approach, but there have been no previous ab initio studies of the O + N_2 reaction.

Section II discusses qualitative features of the reactions studied here. Section III describes the basis sets and computational method, while Section IV discusses the features of the computed potential surfaces. Finally, Section V presents the conclusions.

II. Qualitative Features of the Reactions

First we consider the N + O_2 → NO + O reaction. In C_s symmetry, which is appropriate for the description of the NOO potential energy surface, the ground state reactants N + O_2 have $^4A''$ and $^2A''$ symmetry, respectively (without considering spin-orbit coupling). Thus, $N(^4S)$ and $O_2(^3\Sigma_g^-)$ collisions can occur on $^6A'$, $^4A'$, and $^2A'$ potential energy surfaces with statistical weights of 6/12, 4/12, and 2/12, respectively. Similarly, the ground electronic state products have $^2A'$ and $^2A''$ ($NO\ X^2\Pi$) and $^3A'$ and $^3A''$ ($O\ ^3P$) symmetries. Thus, two sets of $^4A'$,

$^4A''$, $^2A'$, and $^2A''$ potential surfaces lead to the lowest product asymptote. Only the lowest $^4A'$ and $^2A'$ potential energy surfaces connect the lowest reactant and product asymptotes and only they are considered further in this work.

In a localized orbital description the ground state of the O_2 molecule is represented as:

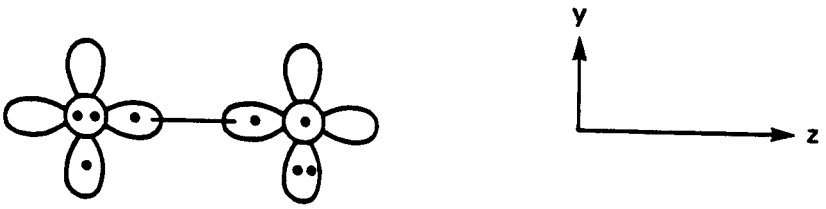

(1)

As discussed elsewhere[9] there is a second equivalent structure and resonance interactions between these two structures result in delocalization of the doubly-occupied π orbitals, so that the π_x and π_y orbitals are equivalent, leading to a $^3\Sigma_g^-$ ground state with the valence configuration (in terms of real orbitals with the atoms lying on the z axis):

$$2\sigma_g^2 2\sigma_u^2 3\sigma_g^2 1\pi_{xu}^2 1\pi_{xg}^1 1\pi_{yu}^2 1\pi_{yg}^1 \qquad (2)$$

Here the $2\sigma_g$ and $2\sigma_u$ orbitals, which are not shown in (1), are derived from the O2s orbitals. The remaining orbitals, which are shown in (1), are the $3\sigma_g$ orbital which is the OOσ bonding orbital(derived from atomic 2pσ), and the π orbitals, which are derived from atomic $2p_x$ and $2p_y$. First consider bringing up a hydrogen atom to (1) to form the ground $^2A''$ state of HO_2. Since H-O_2 bond formation requires localization of the π orbitals as in (1), the HO bond energy is partially cancelled by loss of π bonding for O_2 and there is the possibility of a barrier to H atom addition. POL-CI calculations[9] give a small barrier of 0.4 kcal/mole, although it was predicted that a more complete calculation would lead to no barrier. From (1) it is clear that the optimal angle of approach will involve θ_{HOO} greater than 90°, since the bond pair formed between the H1s and the in plane singly-occupied O2p orbital in (1) must remain orthogonal to the doubly-occupied in-plane O2p orbital on the other O atom.

Bringing up a ^4S N atom to O_2 leads to the asymmetric NOO species shown in (3):

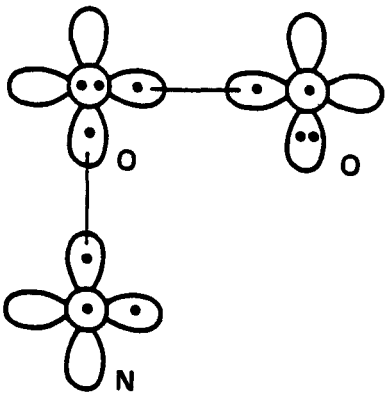

(3)

As for H + O_2 the angle of approach will be greater than 90°. However, the N + O_2 reaction is expected to have a larger entrance channel barrier than the H + O_2 reaction because, upon bond formation, there is a loss of exchange interactions for the high-spin N atom in addition to the loss of π bonding for the O_2 molecule. In addition to the two sigma bonds shown in (3), the two singly-occupied $2p_x$ orbitals may be either singlet or triplet paired leading to $^2A'$ and $^4A'$ surfaces, respectively. The singlet pairing of these orbitals is energetically favored leading to a smaller barrier height for the $^2A'$ surface as compared to the $^4A'$ surface. Since the N + O_2 reaction is exoergic by 32 kcal/mole, we expect an early barrier similar in electronic structure to N + O_2 for the lowest $^2A'$ and $^4A'$ potential energy surfaces. Moving along the reaction coordinate, r_{NO} decreases and r_{OO} increases leading to the breaking of the $OO\sigma$ bond and simultaneous formation of the in plane π bond of the product NO molecule as shown in (4).

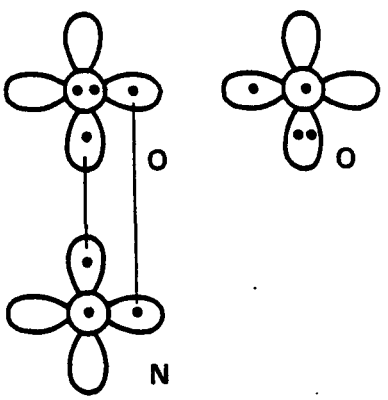

(4)

Because of the energetic nature of the reaction, we do not expect the asymmetric NOO to be a stable species, but rather we expect and find(see section IV) that the energy decreases monotonically moving along the reaction coordinate from the entrance channel saddle point to products.

Next we consider the O + N_2 → NO + N reaction. Because this reaction is endoergic by 75 kcal/mole any barrier is expected to resemble NO + N. Thus, in the following discussion we consider the reaction from the reverse direction, and in fact the calculations have focused largely on the NO + N channel.

Combining the N ^{4}S state with the two components of the $^2\Pi$ state of NO leads to ^{5}A′, ^{5}A″, ^{3}A′, and ^{3}A″ surfaces in C_s symmetry. However, O^{3}P + N_2 $^1\Sigma_g^+$ results in only ^{3}A′ and ^{3}A″ surfaces. In the present study only the latter two surfaces which connect ground state reactants and ground state products are considered. The electronic structures of the NO + N asymptote for the ^{3}A″ and ^{3}A′ surfaces are shown in (5) and (6), respectively.

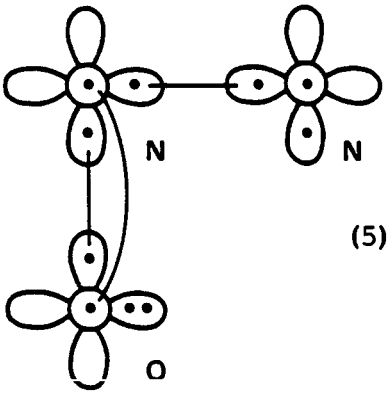

(5)

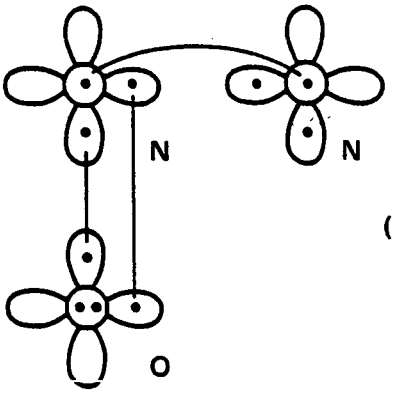

(6)

Here one sees that on the ^{3}A″ surface an initial NNσ bond forms as N and NO approach, while an initial NNπ bond forms on the ^{3}A′ surface. Since σ overlaps are larger than π overlaps, the ^{3}A″ surface will have a smaller barrier than the ^{3}A′ surface. In fact one expects and finds(see section IV) that the ^{3}A″ surface has essentially no barrier while the ^{3}A′ surface has a significant one. As in the N + O_2 case, the entrance channel barriers for these reactions result from the loss of exchange interactions for the high-spin N(^{4}S) atom as well as localization of the NO π orbitals.

The electronic structures for N_2 + O on the ^{3}A″ and ^{3}A′ surfaces are shown in (7) and (8), respectively. Here it is seen that product formation requires breaking NO σ and π bonds with simultaneous formation of two NN π bonds for the ^{3}A″ surface, while NO π and σ bonds are broken with simultaneous formation of an NN σ and π bond for the ^{3}A′ surface. More detailed descriptions of the changes in the bonding occuring during these reactions are given in section IV.

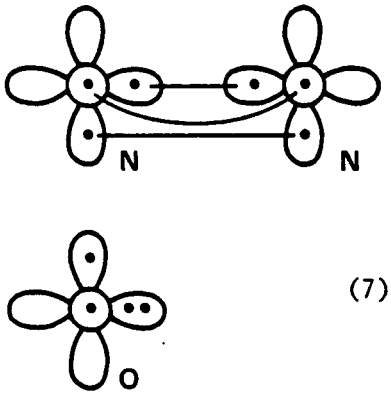

(7)

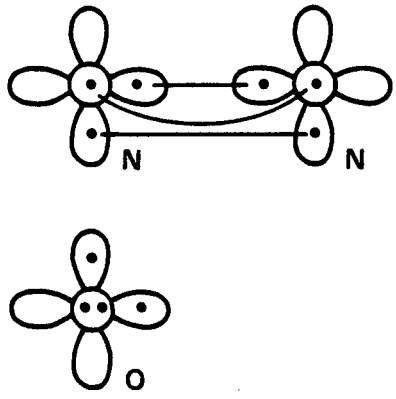

(8)

III. Computational Details

Two different N and O basis sets were used. In both cases the sp basis sets were a [5s3p] segmented contraction of the van Duijneveldt (11s6p) primitive set[10]. The inner nine primitive functions were contracted (63) based on the 1s orbital, while the outer five s functions were contracted (311) based on the 2s orbital. (Note that this contraction uses three functions twice.) The first basis set was augmented by two sets of primitive 3d functions on each atom. The exponents were obtained by optimizing the scale factor for a two term GTO fit[11] to a 3d Slater for the ground states of the atoms at the SDCI level. The resulting two term GTO was then used uncontracted. The exponents used were 1.62 and 0.49 for N and 2.27 and 0.68 for O. The second basis set used the same effective Slater exponent for the 3d functions but used a 3 term fit contracted (21). In addition a single set of 4f functions was added as a two term fit[11] to effective Slater exponents of 2.5 and 3.0 for N and O, respectively. The N and O basis sets are given in Tables I and II, respectively.

The calculations consisted of Complete Active Space SCF (CASSCF)[12] followed by multireference Contracted CI (CCI)[13] as described below. The N2s and O2s derived orbitals were inactive in the CASSCF and were not correlated in the CCI. Since the CCI uses only a limited set of reference configurations, the CCI energy is not invariant to a unitary transformation of the CASSCF orbitals among themselves. The CASSCF active orbitals are uniquely defined by a natural orbital transformation of the converged active orbitals, followed by a CASSCF CI in the natural orbital basis to define the important reference configurations. The multireference analog of Davidson's correction[14] was added to the CCI energy at each computed point. The correction used in the CCI is $\Delta E\ (1 - C_0^2)/C_0^2$ which differs slightly from the original Davidson's correction which is $\Delta E\ (1 - C_0^2)$, where ΔE

is the CI energy minus the reference energy and C_0^2 is the square of the coefficient of the reference configuration or the sum of the squares of the coefficients of the reference configurations in the multireference case. Calculations where Davidson's correction have been added are denoted as CCI + Q. The calculations were carried out using the MOLECULE[15]-SWEDEN[16] system of programs.

A. The $N + O_2 \rightarrow NO + O$ Reaction

The ground state configuration of the O_2 molecule was given in (2). In addition to the SCF orbitals given in (2), the $3\sigma_u$ orbital which introduces left-right correlation of the sigma bond pair is also included in the CASSCF calculations. The ground state of NO is $^2\Pi$ the two components of which are:

$$3\sigma^2 4\sigma^2 5\sigma^2 1\pi_y^2 1\pi_x^2 2\pi_y^1 \tag{9}$$

and

$$3\sigma^2 4\sigma^2 5\sigma^2 1\pi_y^2 1\pi_x^2 2\pi_x^1 \tag{10}$$

Here the 3σ and 4σ orbitals are derived from the O2s and N2s levels, the 5σ is an NOσ bond orbital, and the π orbitals are derived from the N2pπ and O2pπ levels. The CASSCF wave function also includes a 6σ orbital which introduces left-right correlation of the NOσ bond pair. Note also that both the $2\pi_x$ and $2\pi_y$ orbitals are included to describe both components of the $^2\Pi$ state. Combining the N atom and O_2 molecule 2p orbitals leads to an active space consisting of 7a′ - 12a′ and 1a″ - 3a″. (The first six a′ orbitals here correspond to the 1s and 2s orbitals on O and N which are inactive.) The qualitative character of these orbitals for reactants, saddle point, and products is given in Table III. CASSCF calculations were carried out for the lowest ^{2}A′ and ^{4}A′ surfaces of the $N + O_2$ system using the active space defined above with the restriction that there were 7 electrons in a′ orbitals and 4 electrons in a″ orbitals. These constraints lead to 2142 configurations for the ^{2}A′ and 1404 configurations for the ^{4}A′ state. Two different sets of multireference CCI calculations were carried out using the appropriate CASSCF orbitals. The larger set of reference configurations used includes the configurations needed to describe dissociation of both the NO and OO bonds and is therefore able to provide a consistent description over the entire potential surface. The reference configurations for the CCI calculations were:

$$\begin{pmatrix} 7a'^2 8a'^2 12a'^0 \\ 7a'^1 8a'^2 12a'^1 \\ 7a'^0 8a'^2 12a'^2 \end{pmatrix} \times \begin{pmatrix} 9a'^2 10a'^1 11a'^0 \\ 9a'^1 10a'^1 11a'^1 \\ 9a'^0 10a'^1 11a'^2 \end{pmatrix} \times \begin{pmatrix} 1a''^2 2a''^2 3a''^0 \\ 1a''^2 2a''^1 3a''^1 \\ 1a''^2 2a''^0 3a''^2 \end{pmatrix} \tag{11}$$

$$7a'^2 8a'^1 \times 9a'^2 10a'^1 11a'^1 \times 1a''^1 2a''^2 3a''^1 \tag{12}$$

This reference set includes all the configurations with CI coefficients greater than 0.05 in the CASSCF wave function for the $^2A'$ state. Here the first 27 configurations given by (11) are important in the saddle point region, while the last configuration (12) is important in the N + O_2 asymptotic region. This CCI calculation (denoted by ext. CCI) involves about three million configurations(uncontracted).

Calculations were also carried out with a smaller set of reference configurations consisting of the subset of the configurations above which have no electrons in the 12a′ orbital. The resulting CCI calculation (denoted by CCI) involves approximately one million configurations(uncontracted).

The CCI wavefunction is adequate to describe the reactants and entrance channel saddle point region of the surface, since in these regions the OO bond length is close to that of free O_2, and for this limited region of the surface it is not critically important to include configurations which are needed to break the O-O bond. An analagous CCI wavefunction would also be adequate to describe the product region of the surface. From Table III it is seen that for products, 7a′ and 12a′ describe an NOπ bond, while 9a′ and 11a′ describe the NOσ bond pair. This change in orbital character is no problem for the ext. CCI calculation, since these two pairs are treated equivalently, but for the CCI calculation these two pairs would have to be interchanged to be consistent with the configurations given in (11) and (12). However, CCI calculations were not carried out for the product region for this reaction.

While the CCI wavefunction is adequate in the reactants and products regions, it is clearly not adequate in the intermediate region between the entrance channel saddle point and the products region where both the OO and NO bonds are elon-

gated. In addition, as discussed in section IV, the entrance channel barrier height obtained for CCI is 1.7 kcal/mole higher than for the ext. CCI defined above. In spite of this, it is expected and found that the saddle point location obtained with the CCI is not changed by the ext. CCI and other features of the CCI surface are expected to be reasonably accurate over the limited region of the surface for which this wavefunction is valid. As also discussed in Section IV, calculations were carried out along an approximate minimum energy path using the ext. CCI. The entrance channel saddle point location was determined using the CCI with the [5s3p2d] basis set and subsequent calculations were carried out using the ext. CCI with the [5s3p2d] basis set and the CCI with a larger [5s3p2d1f] basis set as described above. The barrier height was estimated by assuming that the effects of expanding the reference space in the CCI and the effects of expanding the basis set are additive.

For the $^4A'$ surface CCI and ext. CCI calculations were carried out, where the reference configurations consisted of the subset of the configurations used for the $^2A'$ surface which contained three or more open shells.

B. The $O + N_2 \rightarrow NO + N$ Reaction

Here the calculations concentrated on the NO + N channel. The ground state configuration for the two components of the $^2\Pi$ state of NO is given in (9) and (10). The ground state configuration of N_2 is:

$$2\sigma_g^2 2\sigma_u^2 3\sigma_g^2 1\pi_{xu}^2 1\pi_{yu}^2 \qquad (13).$$

In addition to the SCF orbitals given above the CASSCF calculation also includes the $3\sigma_u$ and $1\pi_g$ orbitals which are correlating orbitals for the σ and π bonds, respectively. Combining the ^4S N atom with NO $^2\Pi$ leads to a $^3A''$ surface for (9) and a $^3A'$ surface for (10). The CASSCF active space for these surfaces consists of 7a' - 12a' and 1a'' - 3a''. The qualitative character of the CASSCF orbitals for reactants, saddle point, and products regions of the surface is given in Tables IV and V for the $^3A''$ and $^3A'$ states, respectively. CASSCF calculations were carried out for the $^3A''$ surface with the constraint that there were 7 electrons in a' orbitals and 3 electrons in a'' orbitals, which leads to 2652 configurations. CASSCF calculations were also carried out for the $^3A'$ surface with the constraint that there were 6 electrons in a' orbitals and 4 electrons in a'' orbitals, which leads to 2331

configurations.

CCI calculations were also carried out for both surfaces for the N + NO asymptotic regions and for the saddle point region. As in the N + O_2 study, the 12a′ orbital was not included in the active space for the CCI calculations, since for the limited region of the surface studied it was not necessary to include configurations which dissociate the NOσ bond. The reference configurations for the CCI calculations, which again include all configurations with CI coefficients greater than 0.05 in the CASSCF wave function, were:

$$7a'^2 8a'^2 \times \begin{pmatrix} 9a'^2 10a'^1 11a'^0 \\ 9a'^1 10a'^1 11a'^1 \\ 9a'^0 10a'^1 11a'^2 \end{pmatrix} \times \begin{pmatrix} 1a''^2 2a''^1 3a''^0 \\ 1a''^1 2a''^1 3a''^1 \\ 1a''^0 2a''^1 3a''^2 \end{pmatrix} \tag{14}$$

$$7a'^2 8a'^1 \times 9a'^2 10a'^1 11a'^1 \times 1a''^1 2a''^1 3a''^1 \tag{15}$$

for the $^3A''$ surface, and :

$$7a'^2 \times \begin{pmatrix} 8a'^2 9a'^1 10a'^1 11a'^0 \\ 8a'^1 9a'^1 10a'^1 11a'^1 \\ 8a'^0 9a'^1 10a'^1 11a'^2 \end{pmatrix} \times \begin{pmatrix} 1a''^2 2a''^2 3a''^0 \\ 1a''^2 2a''^1 3a''^1 \\ 1a''^2 2a''^0 3a''^2 \end{pmatrix} \tag{16}$$

$$7a'^2 \times 8a'^1 9a'^1 10a'^1 11a'^1 \times 1a''^1 2a''^2 3a''^1 \tag{17}$$

for the $^3A'$ surface. The CCI calculations in each case involved slightly more than one million configurations(uncontracted).

For the $^3A''$ surface, CCI calculations were also carried out for the N_2 + O asymptotic regions. From Table IV it is seen that for the products, 7a′ and 12a′

describe an NNπ bond, while 9a$'$ and 11a$'$ describe the NNσ bond pair. This change in orbital character requires an interchange of these bond pairs for the product region in order to be consistent with the configurations given in (14) and (15). However, with this change the reactant and product regions are treated equivalently. One point was also computed for N + N + O at large internuclear separation using a high spin supermolecule calculation. This result in conjunction with the calculations for the asymptotic regions enables computation of the D_e of NO and N_2 in a supermolecule calculation. The D_e of NO obtained here was used in conjunction with the D_e of O_2 obtained in an analagous fashion for the N + O_2 surface to compute the heat of reaction for the N + O_2 reaction.

IV. Results and Discussion.

The computed energies for the N + O_2 $^2A'$ and $^4A'$ surfaces and the O + N_2 $^3A'$ and $^3A''$ surfaces are given in the appendix. For the N + O_2 $^2A'$ surface CASSCF calculations were carried out at enough points to define the global potential energy surface which is given in Fig. 1. As indicated earlier, the CCI calculations were carried out for the reactants and entrance channel saddle point regions, while the ext. CCI calculations were carried out along the minimum energy path defined by the CASSCF and CCI surface. For the $^4A'$ surface of N + O_2, CCI calculations were carried out for the saddle point region and one calculation was carried out at the saddle point determined in the CCI using the ext. CCI. For the N_2 + O reaction, CCI calculations were carried out for the reactant, saddle point, and product regions for the $^3A''$ surface and for the NO + N asymptotic and saddle point regions for the $^3A'$ surface. All of the above calculations were carried out with the [5s3p2d] basis set. CCI calculations were also carried out using the larger [5s3p2d1f] basis set for the saddle points and asymptotic (N + O_2 and NO + N) regions for all four surfaces.

A. The O_2, NO, and N_2 Molecules

Spectroscopic constants for the O_2, NO, and N_2 molecules were derived from supermolecule calculations for the N + O_2, NO + N, and O +N_2 limits using CCI with the smaller basis set. In addition, calculations were carried out for the above diatomic molecules using both basis sets. For the smaller basis set, the supermolecule calculations differ from the molecular calculations in that they have

the σ bond pair doubly-occupied in all reference configurations, while the molecular calculations include as reference configurations products of all excitations within the σ, π_x and π_y spaces which have the correct molecular symmetry(equivalent to the larger set of reference configurations). Thus, these calculations test the effect of the restrictions made on the reference configurations in the smaller reference space CCI calculations. The calculations with the larger basis set in turn test the effect of 4f functions. In addition calculations were carried out for the diatomics with and without correlating the N2s and O2s derived orbitals in order to test the approximation made in the potential surface calculations of not correlating those orbitals. In each case, r_e, ω_e, and D_0 were computed via a Dunham analysis of a quartic energy expansion. Thus, the computed ω_e and D_0 values include corrections for anharmonicity in the potential.

The results are summarized in Table VI. Looking first at the supermolecule CCI results we see that the computed r_e and ω_e values are in excellent agreement with experiment[17], but the D_0 values are consistently too small. The error in D_0 comes from two major sources. The first is the restriction of leaving the diatomic σ bond pair doubly-occupied in all reference configurations. This leads to an error in the binding energy of O_2 of 0.17 eV. The second source of error is the limited basis set. Here we see that the larger basis set increases the binding energy of O_2 by 0.27 eV. At this level of calculation the errors in the computed D_0 are 0.14, 0.05, and 0.16 eV for O_2, NO, and N_2, respectively. For O_2 and N_2 the effect of correlating the O2s and N2s electrons was also examined. Correlating these additional electrons decreases the D_0 by 0.10 eV and 0.41 eV for O_2 and N_2, respectively. The decrease in binding energy when the 2s shell is correlated probably results from size-consistency errors. However, it is clear that calculations with the 2s electrons not correlated lead to better results for the diatomics and thus this approximation is reasonable for the potential surface calculations. Table VI also compares results with the contracted CI to results without contraction (denoted by SDCI). The largest contraction error is 0.08 eV for the D_0 of O_2. This result indicates that the CCI method works well for the systems studied here.

It may also be seen in Table VI that bond lengths and harmonic frequencies obtained at the CASSCF level are accurate but those calculations obtain a smaller

percentage of the binding energy than CASSCF/CCI. From these results we might expect that the geometries and force fields computed from the CASSCF/CCI potential surface will be accurate, but the CASSCF surfaces will have larger barriers than the CCI surfaces. What is actually found is that the CASSCF method gives reasonable geometries and force constants perpendicular to the reaction coordinate, but that the barrier location along the reaction coordinate is shifted for CCI compared to CASSCF. In addition the approximations of restricting the reference space in the supermolecule CCI calculations as well as the omission of 4f functions in the smaller basis set are expected to increase the barrier height since these constraints decrease the diatomic binding energies. These two effects were tested for the potential surface calculation as described above.

B. The $N + O_2 \rightarrow NO + O$ Reaction.

Fig. 1 shows a plot of the $^2A'$ CASSCF surface for the $N + O_2$ system. Along the minimum energy path connecting reactants and products this surface has two saddle points and one local minimum. The first saddle point is in the entrance channel as expected. In this region of the surface, the predominant interaction is between the $O_2 1\pi_{yg}$ orbital and one of the in plane N2p orbitals leading ultimately to formation of an $NO\sigma$ bond pair. In a simple valence bond picture one might expect an NOO angle of 90°, however repulsive interactions with the O_2 $1\pi_{gu}$ orbital lead to a somewhat larger angle of about 110° for the entrance channel saddle point region. There is a significant barrier (best estimate about 10 kcal/mole) which arises from loss of exchange interactions for the high-spin ^4S N atom as well as loss of resonance interactions in the O_2 molecule due to the localization of the π electrons upon NO bond formation. Shortening the NO bond further leads to a bent asymmetric NOO species which is actually a very shallow minimum on the CASSCF surface. This species is unstable relative to NO + 0 and the second very low energy saddle point corresponds to transfering the $OO\sigma$ bond pair to become a π bond for the product NO molecule. As discussed later the shallow minimum on the CASSCF surface disappears for the ext. CCI calculations, leading to a single saddle point in the entrance channel.

An insertion process to form symmetric NO_2 was also considered but there appears to be a large energy barrier for this reaction and we conclude that formation

of transient symmetric NO_2 would not proceed readily from ^{4}S N plus O_2.

Table III gives the qualitative character of the orbitals for reactants, saddle point, and products. Here the 7a′ orbital corresponds to the OOσ bonding orbital and the 8a′ and 1a″ orbitals correspond to the $1\pi_u$ orbitals of O_2. In the reactants and saddle point regions, these orbitals are not substantially changed from free O_2. There are two bonding interactions. The first involves the $O_2 1\pi_{yg}$ orbital and one of the in plane N2p orbitals. The natural orbitals of this bond pair are the 9a′ and 11a′ orbitals, which correspond approximately to: $O_2 1\pi_{yg} \pm$ N2p, respectively. Proceeding to products this bond pair localizes to become the NOσ bond. The other in plane N2p orbital is the 10a′ orbital which remains essentially atomic like in the saddle point region. However, proceeding to products the 7a′ and 10a′ orbitals spin recouple to form the $NO 1\pi_y$ bond pair and a 2p orbital on the product oxygen atom. The second bond in the saddle point region involves the $O_2 1\pi_{xg}$ and the $N2p_x$ orbitals. The natural orbitals of this bond pair are the 2a″ and 3a″ orbitals, which correspond approximately to: $O_2 1\pi_{xg} \pm N2p_x$, respectively. The a″ pair is only weakly bonding (biradical like) and relocalizes to the singly-occupied $NO 2\pi_x$ and $O2p_x$ orbitals for products. At the same time that these changes are occuring the 8a′ orbital localizes on the product O atom and the 1a″ orbital localizes on the NO to become the $1\pi_x$ orbital.

Given the weak coupling of the a″ pair in the saddle point region the ^{4}A′ CASSCF natural orbitals are very similar to those of the ^{2}A′ surface. Loss of the a″ bonding interactions leads to a barrier for the ^{4}A″ surface about 8 kcal/mole higher than the doublet surface. At low temperatures the rate constant will be controlled primarily by the ^{2}A′ surface, owing to the lower barrier to reaction, but at higher temperatures both the ^{2}A′ and ^{4}A′ surfaces will be important with the ^{4}A′ surface having twice the statistical weight of the ^{2}A′ surface.

In order to locate the saddle points for the ^{2}A′ and ^{4}A′ surfaces, grids of points were computed in r_{NO} and r_{OO} for an NOO angle of 110° using the smaller basis set at the CCI level. This angle was estimated from preliminary CASSCF calculations; it was subsequently varied about the saddle point obtained for a fixed angle of 110° and was found to be very close to the optimal value. The saddle point on the r_{NO} and r_{OO} grid was obtained from a fit of the energies to a quadratic polynomial of

the form:

$$E(r_{NO}, r_{OO}) = c_1 + c_2 r_{NO} + c_3 r_{OO} + c_4 r_{NO} r_{OO} + c_5 r_{NO}^2 + c_6 r_{OO}^2 \qquad (18)$$

To this polynomial was added a quadratic term in the NOO angle and the vibrational frequencies at the saddle point were obtained from this energy expression using the conventional F and G matrix method[18]. Calculations were also carried out using the larger basis set at the CCI level and using the smaller basis set at the ext. CCI level. The results are given in Table VII. Here for the $^2A'$ surface it is seen that at the CCI + Q level with the smaller basis set the computed barrier is 13.4 kcal/mole. The larger basis set reduces the barrier by 1.5 kcal/mole, while the ext. CCI reduces the barrier by 1.7 kcal/mole. Combining these two effects leads to 10.2 kcal/mole as our best estimate of the barrier. From Table VII it is seen that the saddle point location with the ext. CCI is very similar to the saddle point location obtained with the CCI. Table VII also shows the saddle point vibrational frequencies and computed zero point correction. The zero point correction is +0.44 kcal/mole leading to an effective barrier of 10.6 kcal/mole. This number may be compared to an experimental activation energy of 6-8 kcal/mole[6,19] which suggests that the computed barrier is too large by at least 2-3 kcal/mole. At least part of this error results from basis set effects, since for the O + H_2 reaction, addition of a third d, a second f, and a g function to the O basis set used in these studies in conjunction with improvements in the H basis set lowered the barrier height by more than 1.0 kcal/mole[20]. There may also be some remaining differential effect due to higher excitations. The Davidson's correction at the saddle point geometry is 0.023 hartree, while the differential Davidson's correction between reactants and saddle point is 2.9 kcal/mole for the ext. CCI. These results indicate that higher excitations are still significant for the highest level of correlation treatment considered here and may account for a large part of the remaining error in the barrier height. The computed saddle point geometry has an NOO angle of 115°. The bending potential about the saddle point geometry is shown in Fig. 2.

Table VII also shows the results for the CASSCF calculations. Here it is seen that the barrier height is about 8 kcal/mole larger than the best CCI result using the same basis set. Also, the saddle point is shifted somewhat toward shorter r_{NO}. These results are consistent with the conclusion, deduced from studies of the O +

H_2[21] and OH + H_2[22] reactions, that MCSCF wave functions give consistently high barriers. Table VII also shows the calculated exoergicity for the reaction. Here CCI + Q gives 30.9 kcal/mole while CASSCF gives 35.0 kcal/mole, compared to the experimental value of 32 kcal/mole[17].

Table VIII shows computed energies along the minimum energy path for the N + O_2 reaction on the CASSCF, CCI, and ext. CCI $^2A'$ surfaces. These minimum energy paths were obtained from the CASSCF surface by interpolation on the rectangular grid of CASSCF and CCI energies computed for an angle of 110°. In the intermediate region this corresponds to a rotated Morse oscillator description with a pivot point at $r_{NO} = 2.9$ and $r_{OO} = 3.1$. For r_{NO} greater than 2.9 and r_{OO} greater than 3.1 the reaction coordinate is approximately r_{OO} and r_{NO}, respectively. One interesting feature of Table VIII is that the shallow minimum corresponding to an asymmetric NOO structure on the CASSCF surface disappears at the ext. CCI level.

A similar treatment was carried out for the $^4A'$ surface. The resulting saddle point geometry is given in Table VII, while the bending potential is shown in Fig. 2 and the minimum energy paths at both the CASSCF and CCI + Q level are given in Table IX. Additional calculations were carried out at the saddle point geometry which was obtained with the smaller basis set and smaller set of reference configurations using i) CCI with the larger basis set and ii) ext. CCI with the smaller basis set. These results are also given in Table VII. Here it is seen that the larger basis set lowers the barrier by 1.5 kcal/mole, while the ext. CCI lowers the barrier by 1.1 kcal/mole. Combining these two effects leads to 18.0 kcal/mole as the best estimate of the barrier, although based on the $^2A'$ surface we expect that this barrier is still too large by 2-3 kcal/mole. Other than the larger barrier height, the general features of this surface are similar to those of the $^2A'$ surface.

C. The O + N_2 → NO + N Reaction.

Calculations were carried out for both the $^3A''$ and $^3A'$ surfaces. The calculations focused primarily on the NO + N channel. Table IV shows the qualitative nature of the orbitals for the $^3A''$ surface of the N + NO reaction for reactants, saddle point, and products. Here the 7a′ orbital corresponds to the NOσ bond pair, the 8a′ and 1a″ orbitals correspond to the two components of the NO1π orbital. There is one

bond pair formed between the NO2π orbital and one of the in plane N2p orbitals. The natural orbitals of this bond pair are the 9a$'$ and 11a$'$ orbitals which correspond approximately to: NO2π_y $\pm$ N2p, respectively. This bond pair becomes the NNσ bond pair for the products. The remaining orbitals are the 2a$''$ and the 10a$'$ which are atomic N2p like. To go to the N_2 + O products requires spin recoupling of the 7a$'$ and 10a$'$ orbitals to form one π bond with simultaneous spin recoupling of the 1a$''$ and 2a$''$ orbitals to form the other π bond of N_2.

Table V shows the qualitative nature of the orbitals for the ^{3}A$'$ surface for the reactants, saddle point, and products regions. Here the 7a$'$ orbital corresponds to the NO σ bond pair, and the 8a$'$ and 1a$''$ orbitals correspond to the two components of the NO1π orbital. The 11a$'$ orbital is a correlating orbital for the in plane NOπ orbital, and the 9a$'$ and 10a$'$ orbitals are N2p orbitals. There is one bond pair formed between the NO2π orbital and the N2p$_x$ orbital. The natural orbitals of this bond pair are the 2a$''$ and 3a$''$ orbitals which correspond approximately to: NO2π_x $\pm$ N2p$_x$, respectively. This bond pair becomes an NNπ bond pair for the products. To go to the N_2 + O limit requires spin recoupling of the 8a$'$ and 9a$'$ orbitals to form the NNσ bond, with simultaneous spin recoupling of the 7a$'$ and 10a$'$ orbitals to form the other NNπ bond.

The ^{3}A$''$ surface has a very small barrier which occurs for large r_{NN}, while the ^{3}A$'$ surface has a substantial barrier which occurs for smaller r_{NN}. For both surfaces, grids of points in r_{NN} and r_{NO} were computed for a fixed θ_{NNO} of 110°. θ_{NNO} was then varied about the approximate saddle point position and the resulting bending curves are shown in Fig. 3.

Table X summarizes the computed potential surface properties for the O + N_2 reaction. The CCI results with the larger basis set yielded computed barriers of 0.5 kcal/mole for ^{3}A$'$ and 14.4 kcal/mole for ^{3}A$''$. In both cases the zero point corrections are positive leading to corrected barrier heights of 1.0 kcal/mole and 14.7 kcal/mole, respectively. It is likely that further improvement in the calculation would lead to no barrier for the ^{3}A$''$ surface. The computed endoergicity for this reaction is 77.0 kcal/mole at the CCI + Q level and 80.6 kcal/mole at the CASSCF level compared to an experimental value of 75 kcal/mole[17].

Tables XI and XII show the computed minimum energy paths for both CASSCF

and CCI + Q calculations of the $^3A''$ and $^3A'$ surfaces, respectively. These results are plotted in Fig. 4. As noted for N + O_2, the CASSCF calculation leads to too large a barrier height and shifted saddle point locations relative to the CCI + Q surface. As discussed earlier the differences between the $^3A'$ and $^3A''$ surfaces result from the different strengths of the initial N-NO bond. For the $^3A'$ surface the NNπ bond is too weak to compensate for loss of exchange interactions for the high-spin N(^{4}S) atom. Thus, the saddle point occurs for shorter atom-diatom distances and has a higher barrier for the $^3A'$ surface. From these results we expect that, even at fairly high temperatures, the reverse reaction i.e. N + NO $\rightarrow$ N_2 + O will occur almost entirely on the $^3A''$ surface.

V. Conclusions.

CASSCF/CCI calculations have been carried out for the $^2A'$ and $^4A'$ surfaces for the N + O_2 $\rightarrow$ NO + O reaction and for the $^3A'$ and $^3A''$ surfaces for the O + N_2 $\rightarrow$ NO + N reaction.

The N + O_2 reaction is exoergic by 32 kcal/mole, which leads to an early barrier of 10.2 kcal/mole for the $^2A'$ surface. The computed barrier height is about 3 kcal/mole larger than the experimental activation energy of 7-8 kcal/mole, after consideration of zero point energy differences. The $^4A'$ surface has a larger barrier, 18.0 kcal/mole.

The O + N_2 reaction is endoergic by 75 kcal/mole and is computed to have approximately a 1.0 kcal/mole additional energy barrier (resembling NO + N). However, considering the limitations of the calculations there is probably no additional barrier. The barrier region to the reverse reaction was considered in detail. Combining N ^{4}S with the two components of the $^2\Pi$ ground state of NO leads to $^3A'$ and $^3A''$ states. The potential surfaces for these two states differ significantly, with the $^3A''$ surface being characterized by a large atom-diatom distance and very small barrier (0.5 kcal/mole), while the $^3A'$ surface has a smaller atom-diatom distance and a large barrier (14.4 kcal/mole). These differences are related to the relative strengths of the initially formed bonds. The $^3A''$ surface initially forms an NNσ bond, while the $^3A'$ surface initially forms a weaker NNπ bond. The stronger NNσ bond in the case of the $^3A''$ surface is better able to compensate for loss of exchange interactions for the high-spin N(^{4}S) atom as compared to the weaker NNπ bond in

the case of the $^3A'$ surface. These qualitative differences imply that reaction of N and NO would occur primarily on the $^3A''$ surface.

ACKNOWLEDGMENTS

S.P. Walch was supported by a NASA grant(NCC2-296).

References

1. E.E. Whiting, J.O. Arnold, W.A. Page, and R.M. Reynolds, J. Quant. Spectroscopy and Radiative Transfer, **13**, 837(1973).
2. C. Park, in "Thermal Design of Aeroassisted Orbital Transfer Vehicles", edited by H.F. Nelson, Vol. 96 of Progress in Astronautics and Aeronautics, 1985, pp. 511-537.
3. R.L. Jaffe, "Rate Constants for Chemical Reactions in High-Temperature Non-Equilibrium Air", paper no. AIAA-85-1038, 20th Thermophysics Conference, Williamsburg, Va., June 19-21, 1985.
4. J.R. Stallcop and H. Partridge, Phys. Rev. A, **32**, 639(1985).
5. H. Partridge and S.R. Langhoff, to be published.
6. D.L. Baulch, D.D. Drysdale, D.G. Horn, and A.C. Lloyd, "Evaluated Kinetic Data for High Temperature Reactions, Vol 2., Homogeneous Gas Phase Reactions of the H_2-N_2-O_2 System", Chemical Rubber Co. Press, Cleveland, 1973.
7. J. Blauwens, B. Smets, and J. Peeters, Sixteenth Symposium (International) on Combustion, p. 1055, The Combustion Institute, 1976, and references therein.
8. G. Das and P.A. Benioff, Chem. Phys. Lett., **75**, 519(1980).
9. T.H. Dunning,Jr., S.P. Walch, and M.M. Goodgame, J. Chem. Phys., **74**, 3482(1981).
10. F.B. van Duijneveldt, IBM Technical Research Report No. RJ945 (1971).
11. R.F. Stewart, J. Chem. Phys., **52**, 431(1970).
12. P.E.M. Siegbahn, A. Heiberg, B. Roos, and B. Levy, Physica Scripta, **21**, 323(1980).
13. P.E.M. Siegbahn, Int. J. of Quantum Chem., **23**,1869(1983).
14. S.R. Langhoff and E.R. Davidson, Int. J. of Quantum Chem., **8**, 61(1974).
15. J. Almlöf, MOLECULE, a Gaussian integral program.
16. P.E.M. Siegbahn, C.W. Bauschlicher,Jr., B. Roos, A. Heiberg, P.R. Taylor, and J. Almlöf, SWEDEN, A vectorized SCF MCSCF direct CI.

17. K.P. Huber and G. Herzberg, "Molecular Spectra and Molecular Structure",(Van Nostrand Reinhold, New York, 1979.)

18. E.B. Wilson, Jr., J.C. Decius, and P.C. Cross, Molecular Vibrations: The Theory of Infrared and Raman Vibrational Spectra, McGraw-Hill, New York, 1955.

19. R.R. Herm, B.J. Sullivan, and M.E. Whitson,Jr., J. Chem. Phys., **79**, 2221(1983).

20. S.P. Walch, J. Chem. Phys., to be published.

21. S.P. Walch, T.H. Dunning,Jr., R.C. Raffenetti, and F.W. Bobrowicz, J. Chem. Phys., **72**, 406(1980).

22. S.P. Walch and T.H. Dunning,Jr., J. Chem. Phys., **72**, 1303(1980).

Table I. Basis Sets for Nitrogen.

N [5s3p] valence basis

function	s	p
1	22800.200(0.00022)	49.3707(0.00553)
2	3413.4500(0.00172)	11.3801(0.03791)
3	776.38300(0.00891)	3.43690(0.14903)
4	219.96600(0.03602)	1.18210(0.34890)
5	71.795200(0.11551)	0.41746(1.00000)
6	25.817500(0.27756)	0.14285(1.00000)
7	9.9295400(0.42314)	
8	3.9484300(0.27113)	
9	1.1108500(0.02441)	
7	9.9295400(-.14304)	
8	3.9484300(-.14193)	
9	1.1108500(0.24422)	
10	0.436520(1.00000)	
11	0.160920(1.00000)	

[2d1f] polarization basis

function	d	f
1	3.0620(0.16866)	1.254(0.47694)
2	0.9600(0.58480)	0.429(0.65874)
3	0.3740(1.00000)	

Table II. Basis Sets for Oxygen.

O [5s3p] valence basis

function	s	p
1	31195.560(0.00021)	64.7719(0.00584)
2	4669.3800(0.00163)	14.9727(0.04058)
3	1062.2600(0.00845)	4.55440(0.15754)
4	301.42600(0.03419)	1.56370(0.35300)
5	98.515300(0.11031)	0.54107(1.00000)
6	35.460900(0.26949)	0.17776(1.00000)
7	13.617900(0.42355)	
8	5.3862000(0.28304)	
9	1.5387000(0.02748)	
7	13.617900(-.14601)	
8	5.3862000(-.14788)	
9	1.5387000(0.23867)	
10	0.605500(1.00000)	
11	0.220500(1.00000)	

[2d1f] polarization basis

function	d	f
1	4.2770(0.16866)	1.806(0.47694)
2	1.3410(0.58480)	0.618(0.65874)
3	0.5220(1.00000)	

Table III. Qualitative Character of the CASSCF Orbitals for $N + O_2 \rightarrow NO + O$, $^{2,4}A'$ Surface

orbital	reactants	saddle point	products
7a′	$O_2 3\sigma_g$	$O_2 3\sigma_g$	$NO 1\pi_y$
8a′	$O_2 1\pi_{yu}$	$O_2 1\pi_{yu}$	$O 2p_y$
9a′	$O_2 1\pi_{yg}$	$O_2 1\pi_{yg} + N 2p_y$	$NO 5\sigma$
10a′	$N 2p_z$	$N 2p_z$	$O 2p_z$
11a′	$N 2p_y$	$O_2 1\pi_{yg} - N 2p_y$	$NO 6\sigma$
12a′	$O_2 3\sigma_u$	$O_2 3\sigma_u$	$NO 2\pi_y$
1a″	$O_2 1\pi_{xu}$	$O_2 1\pi_{xu}$	$NO 1\pi_x$
2a″	$O_2 1\pi_{xg}$	$O_2 1\pi_{xg} + N 2p_x$	$NO 2\pi_x + O 2p_x$
3a″	$N 2p_x$	$O_2 1\pi_{xg} - N 2p_x$	$NO 2\pi_x - O 2p_x$

Table IV. Qualitative Character of the CASSCF Orbitals for $NO + N \rightarrow N_2 + O$, $^3A''$ Surface

orbital	reactants	saddle point	products
7a′	NO5σ	NO5σ	$N_2 1\pi_{yu}$
8a′	NO1π_y	NO1π_y	O2p_z
9a′	NO2π_y	NO2π_y + N2p_z	$N_2 3\sigma_g$
10a′	N2p_y	N2p_y	O2p_y
11a′	N2p_z	NO2π_y − N2p_z	$N_2 3\sigma_u$
12a′	NO6σ	NO6σ	$N_2 1\pi_{yg}$
1a″	NO1π_x	NO1π_x	$N_2 1\pi_{xu}$
2a″	N2p_x	N2p_x	O2p_x
3a″	NO2π_x	NO2π_x	$N_2 1\pi_{xg}$

Table V. Qualitative Character of the CASSCF Orbitals for $NO + N \rightarrow N_2 + O$, $^3A'$ Surface

orbital	reactants	saddle point	products
7a′	NO5σ	NO5σ	$N_2 1\pi_{yu}$
8a′	NO1π_y	NO1π_y	$N_2 3\sigma_g$
9a′	N2p$_z$	N2p$_z$	O2p$_z$
10a′	N2p$_y$	N2p$_y$	O2p$_y$
11a′	NO2π_y	NO2π_y	$N_2 3\sigma_u$
12a′	NO6σ	NO6σ	$N_2 1\pi_{yg}$
1a″	NO1π_x	NO1π_x	O2p$_x$
2a″	N2p$_x$	NO2π_x + N2p$_x$	$N_2 1\pi_{xu}$
3a″	NO2π_x	NO2π_x − N2p$_x$	$N_2 1\pi_{xg}$

Table VI. Computed Spectroscopic Constants for O_2, NO, and N_2[a].

		O_2			NO			N_2		
		r_e	ω_e	D_0	r_e	ω_e	D_0	r_e	ω_e	D_0
[5s3p2d]	CCI + Q	2.291	1580	4.537	2.176	1926	5.877	2.076	2381	9.187
supermolecule	CASSCF	2.307	1522	3.634	2.185	1894	5.150	2.083	2359	8.618
[5s3p2d]	CCI + Q			4.702						
	SDCI + Q			4.783						
	CCI + Q + 2s			4.598						
[5s3p2d1f]	CCI + Q			4.973			6.443	2.078	2383	9.595
	SDCI + Q									9.602
	CCI + Q + 2s									9.190
Experiment		2.282	1580	5.116	2.175	1904	6.497	2.704	2359	9.759

[a] r_e in a_0, ω_e in cm^{-1}, and D_0 in eV.

Table VII. Computed Potential Surface Properties for $N + O_2 \rightarrow NO + O$[a].

		$^2A'$		$^4A'$	
		CCI + Q	CASSCF	CCI + Q	CASSCF
ΔE_{rx}^b	[5s3p2d]	−30.9	−35.0	−30.9	−35.0
ΔE_b^c	[5s3p2d]	13.4	19.7	20.6	28.4
	[5s3p2d1f]	11.9	18.4	19.1	27.1
	ext. CCI	11.7		19.5	
	best estimate	10.2		18.0	
saddle point geometry[d]	r_{NO}	3.441	3.269	3.310	3.154
	r_{OO}	2.329	2.368	2.359	2.434
	θ_{NOO}	115.0	114.1	109.4	109.9
saddle point frequencies	ω_1	1498.	1294.	1406.	1187.
	ω_2	370.	367.	367.	365.
	ω_3	505. i	702. i	689. i	612. i
zero point correction		0.44	0.13	0.30	−.02
corrected ΔE_b		10.6	18.5	18.3	27.1

[a] Energy quantities are in kcal/mole and geometries are in a_0.
[b] Heat of Reaction. The heat of reaction for $N + O_2$ was obtained from the supermolecule D_e's for O_2 and NO given in Table VI.
[c] Barrier Height.
[d] Using the ext. CCI the saddle point location for $\theta = 110°$ is $r_{NO} = 3.433$ and $r_{OO} = 2.354$. The barrier height at this saddle point location is 11.76 kcal/mole.

Table VIII. Minimum Energy Path for $N + O_2 \rightarrow NO + O$, $^2A'$ surface.[a,b]

CASSCF			CCI + Q			Ext. CCI + Q		
r_{NO}	r_{OO}	Energy	r_{NO}	r_{OO}	Energy	r_{NO}	r_{OO}	Energy
20.0	2.313	-204.15389	20.0	2.295	-204.35700	20.0	2.291	-204.36861
3.70	2.332	-204.13030	3.70	2.299	-204.33777	3.70	2.299	-204.35202
3.50	2.344	-204.12516	3.50	2.326	-204.33588	3.50	2.326	-204.34991
3.30	2.365	-204.12247	3.30	2.344	-204.33660	3.30	2.344	-204.35025
3.10	2.408	-204.12370	3.10	2.371	-204.34160	3.10	2.371	-204.35479
2.90	2.452	-204.13084	2.90	2.412	-204.34959	2.90	2.412	-204.36351
2.687	2.444	-204.14017				2.687	2.444	-204.37579
2.449	2.507	-204.14740				2.449	2.507	-204.38615
2.378	2.572	-204.14797				2.378	2.572	-204.38873
2.300	2.737	-204.14718				2.300	2.737	-204.39437
2.206	2.998	-204.15806				2.206	2.998	-204.39738
2.205	3.50	-204.18523						
2.218	4.00	-204.19868						

[a] $\theta_{NOO} = 110°$

[b] All quantities are in atomic units.

Table IX. Minimum Energy Path for $N + O_2 \rightarrow NO + O$, $^4A'$ Surface[a,b]

CASSCF			CCI + Q		
r_{NO}	r_{OO}	Energy	r_{NO}	r_{OO}	Energy
20.0	2.313	-204.15389	20.0	2.295	-204.35700
3.50	2.350	-204.11602	3.50	2.331	-204.32602
3.30	2.382	-204.10961	3.30	2.361	-204.32602
3.10	2.454	-204.10863	3.10	2.415	-204.32544
2.90	2.516	-204.11190	2.90	2.466	-204.32991

[a] $\theta_{NOO} = 110°$

[b] All quantities are in atomic units.

Table X. Computed Potential Surface Properties for $N + NO \rightarrow N_2 + O$

		$^3A''$		$^3A'$	
		CCI + Q	CASSCF	CCI + Q	CASSCF
ΔE_{rx}^b	[5s3p2d]	-77.0	-80.6	-77.0	-80.6
ΔE_b^c	[5s3p2d]	1.3	7.6	16.6	28.1
	[5s3p2d1f]	0.5	5.0	14.4	25.3
saddle point	r_{NN}	4.102	3.438	3.574	3.324
geometry	r_{NO}	2.172	2.197	2.210	2.250
	θ_{NNO}	108.9	108.5	116.5	116.5
saddle point	ω_1	1785.	1720.	1678.	1586.
frequencies	ω_2	385.	396.	383.	383.
	ω_3	210. i	250. i	569. i	727. i
zero point correction		0.47	0.39	0.31	0.18
corrected ΔE_b		1.0	5.4	14.7	25.5

[a] Energy quantities are in kcal/mole and geometries are in a_0.
[b] Heat of Reaction.
[c] Barrier Height.

Table XI. Minimum Energy Path for $N + NO \rightarrow N_2 + O$, $^3A''$ surface[a,b]

CASSCF			CCI + Q		
r_{NN}	r_{NO}	Energy	r_{NN}	r_{NO}	Energy
20.0	2.192	-183.80080	20.0	2.182	-183.95325
4.50	2.189	-183.79601	4.50	2.177	-183.95185
4.00	2.187	-183.79171	4.00	2.174	-183.95113
3.50	2.197	-183.78875	3.50	2.188	-183.95384
3.00	2.243	-183.79137	3.00	2.242	-183.96240

[a] $\theta_{NNO} = 110°$

[b] All quantities are in atomic units.

Table XII. Minimum Energy Path for N + NO → N_2 + O, $^3A'$ surface[a,b]

CASSCF			CCI + Q		
r_{NN}	r_{NO}	Energy	r_{NN}	r_{NO}	Energy
20.0	2.20	-183.80109	20.0	2.20	-183.95330
4.50	2.192	-183.79096	4.50	2.184	-183.94585
4.00	2.195	-183.77798	4.00	2.187	-183.93577
3.50	2.210	-183.75720	3.50	2.196	-183.92708
3.00	2.264	-183.75941	3.00	2.239	-183.94257

[a] $\theta_{NNO} = 110°$

[b] All quantities are in atomic units.

Figure Captions.

Fig. 1. A plot of the global CASSCF potential surface for the $^2A'$ state of the N + $O_2 \rightarrow$ NO + O reaction.

Fig. 2. Bending potentials for the saddle point region of the $^2A'$ and $^4A'$ surfaces of the N + $O_2 \rightarrow$ NO + O reaction. The bending potentials are shown for both CASSCF and CCI + Q.

Fig. 3. Bending potentials for the saddle point region of the $^3A'$ and $^3A''$ surfaces of the O + $N_2 \rightarrow$ NO + N reaction. The bending potentials are shown for both CASSCF and CCI + Q.

Fig. 4. Energy along the minimum energy path for the $^3A''$ and $^3A'$ surfaces for NO + N for both CASSCF and CCI wave functions.

Fig. 1

$^2A'$ CASSCF POTENTIAL SURFACE FOR $N + O_2 \longrightarrow NO + O$

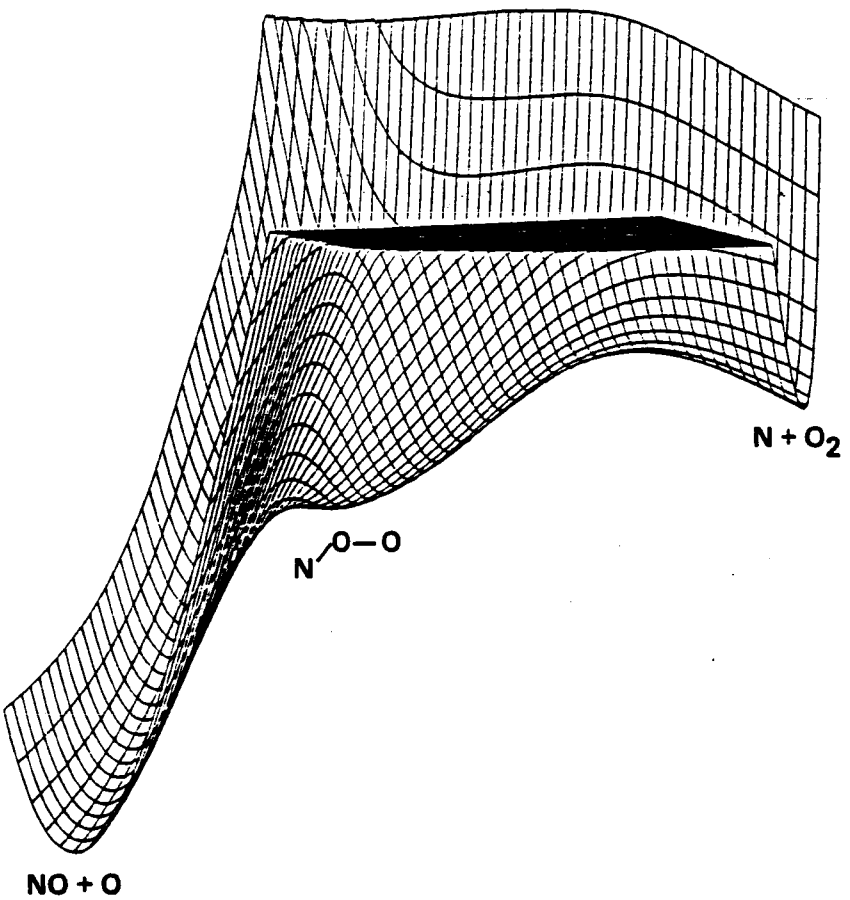

WALCH

Fig. 2

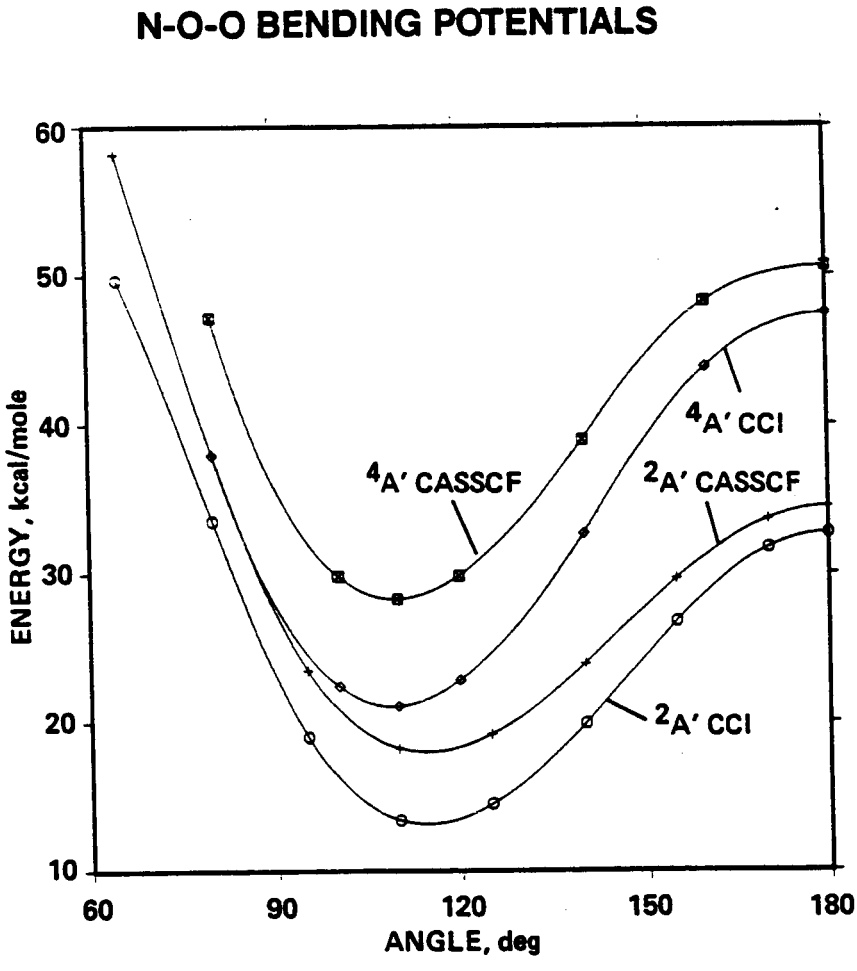
N-O-O BENDING POTENTIALS
ENERGY, kcal/mole
60
50
40
30
20
10
60
90
120
150
180
ANGLE, deg
4A' CASSCF
4A' CCI
2A' CASSCF
2A' CCI

Fig. 3

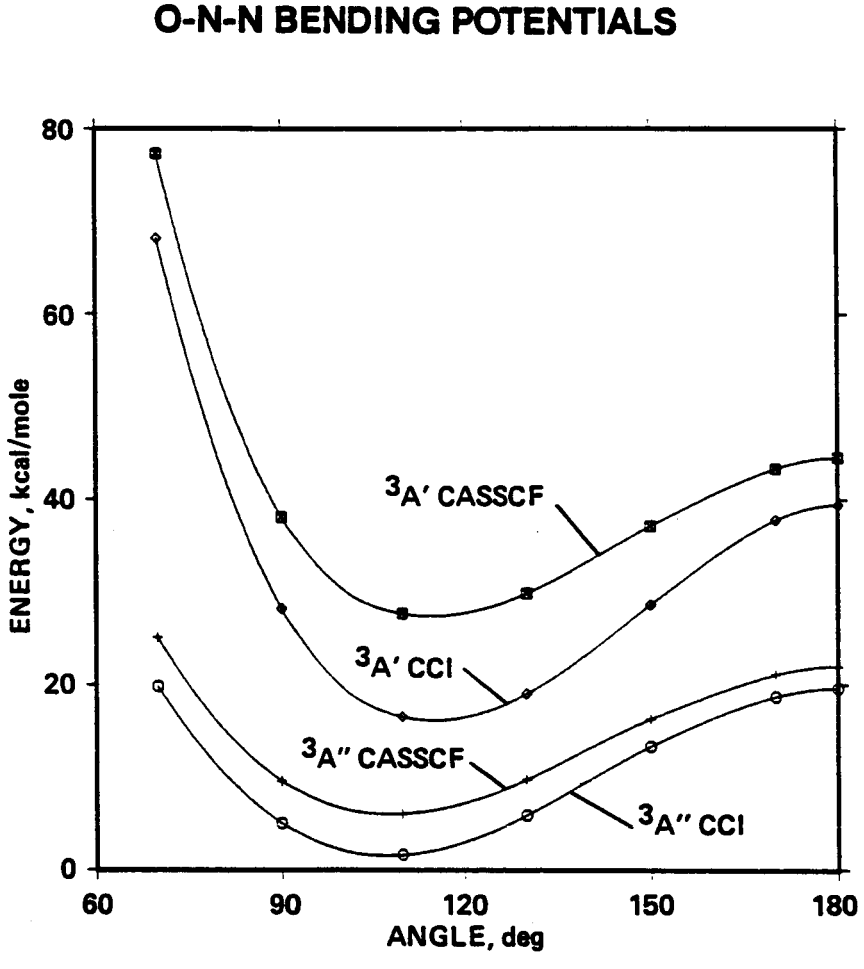
O-N-N BENDING POTENTIALS
80
60
40
20
0
ENERGY, kcal/mole
60
90
120
150
180
ANGLE, deg
^{3}A' CASSCF
^{3}A' CCI
^{3}A" CASSCF
^{3}A" CCI

Fig. 4

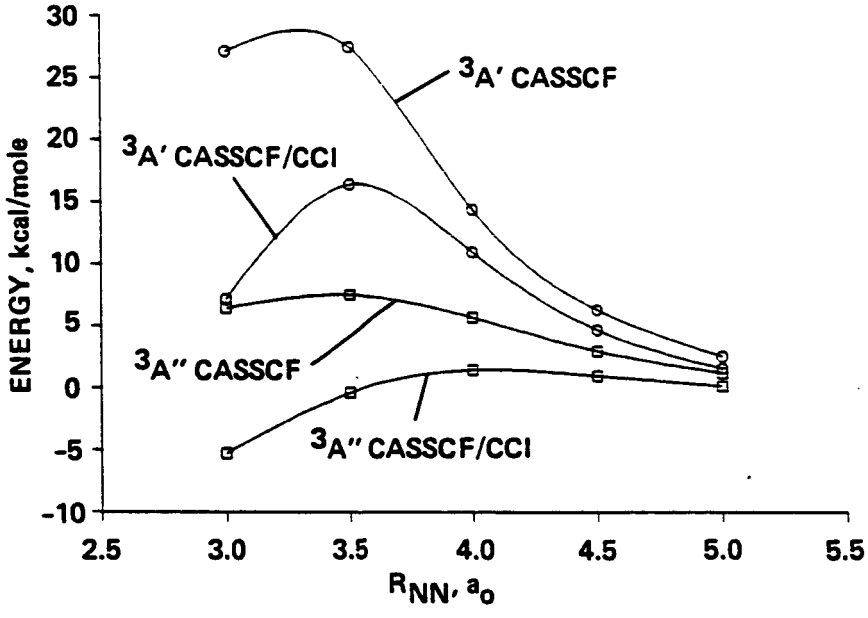
30
25
20
15
10
5
0
-5
-10
ENERGY, kcal/mole
2.5
3.0
3.5
4.0
4.5
5.0
5.5
R_{NN}, a_o
$^3A'$ CASSCF
$^3A'$ CASSCF/CCI
$^3A''$ CASSCF
$^3A''$ CASSCF/CCI

Appendix. The appendix contains tables of the computed energies. In the following tables, all distances and energies are in atomic units and θ is degrees. See the text for a description of the computational method.

Table AI. Energies for The $N + O_2 \rightarrow NO + O$ Reaction

$^2A'$ Surface

θ	r_{NO}	r_{OO}	E(CASSCF)	E(CCI + Q)
110.0	20.000	2.500	-204.14355	-204.34412
110.0	20.000	2.400	-204.15107	-204.35290
110.0	20.000	2.282	-204.15353	-204.35694
110.0	20.000	2.200	-204.14913	-204.35369
110.0	20.000	2.100	-204.13392	-204.34202
110.0	20.000	20.000	-204.01675	-204.18666
110.0	3.700	2.750	-204.09542	-204.29479
110.0	3.700	2.600	-204.11227	-204.31487
110.0	3.700	2.450	-204.12534	-204.32704
110.0	3.700	2.300	-204.12994	-204.33777
110.0	3.700	2.150	-204.11859	-204.32742
110.0	3.700	2.000	-204.07903	-204.29269
110.0	3.500	2.750	-204.09465	-204.29739
110.0	3.500	2.600	-204.10975	-204.31577
110.0	3.500	2.450	-204.12123	-204.33003
110.0	3.500	2.300	-204.12450	-204.33562
110.0	3.500	2.150	-204.11213	-204.32410
110.0	3.500	2.000	-204.07199	-204.28825
110.0	3.300	2.750	-204.09802	-204.30469
110.0	3.300	2.600	-204.11087	-204.32072
110.0	3.300	2.450	-204.12001	-204.33259
110.0	3.300	2.300	-204.12104	-204.33589
110.0	3.300	2.150	-204.10676	-204.32300
110.0	3.300	2.000	-204.06522	-204.28427
110.0	3.100	2.750	-204.10603	-204.31609
110.0	3.100	2.600	-204.11679	-204.33012
110.0	3.100	2.450	-204.12336	-204.33942

110.0	3.100	2.300	-204.12154	-204.33981
110.0	3.100	2.150	-204.10439	-204.32437
110.0	3.100	2.000	-204.06031	-204.28102
110.0	2.900	3.000	-204.09801	
110.0	2.900	2.750	-204.11730	
110.0	2.900	2.600	-204.12646	-204.34208
110.0	2.900	2.450	-204.13084	-204.34929
110.0	2.900	2.300	-204.12622	-204.34689
110.0	2.900	2.150	-204.10579	-204.32818
110.0	2.700	4.000	-204.12817	
110.0	2.700	3.500	-204.11330	
110.0	2.700	3.000	-204.11256	
110.0	2.700	2.750	-204.12945	
110.0	2.700	2.600	-204.13720	
110.0	2.700	2.450	-204.13971	
110.0	2.700	2.400	-204.13869	
110.0	2.700	2.300	-204.13262	
110.0	2.700	2.000	-204.05765	
110.0	2.500	4.000	-204.16464	
110.0	2.500	3.500	-204.14941	
110.0	2.500	3.000	-204.13112	
110.0	2.500	2.800	-204.13819	
110.0	2.500	2.750	-204.14046	
110.0	2.500	2.600	-204.14570	
110.0	2.500	2.450	-204.14581	
110.0	2.500	2.400	-204.14394	
110.0	2.500	2.282	-204.13389	
110.0	2.500	2.000	-204.05365	
110.0	2.200	4.000	-204.19854	
110.0	2.200	3.500	-204.18522	
110.0	2.200	3.000	-204.15834	
110.0	2.200	2.750	-204.14585	

110.0	2.200	2.600	-204.14198	
110.0	2.200	2.450	-204.13436	
110.0	2.200	2.300	-204.11750	
110.0	2.200	2.000	-204.02003	
110.0	2.000	4.000	-204.17823	
110.0	2.000	3.500	-204.16801	
110.0	2.000	3.000	-204.14086	
110.0	2.000	2.750	-204.11848	
110.0	2.000	2.600	-204.10581	
110.0	2.000	2.300	-204.06444	
110.0	2.000	2.000	-203.95082	
130.0	3.300	2.300	-204.11527	
120.0	3.300	2.300	-204.12047	
100.0	3.300	2.300	-204.11561	
90.0	3.300	2.300	-204.10234	
115.0	3.441	2.329	-204.12389	-204.33567
180.0	3.500	2.300	-204.09866	-204.30487
170.0	3.500	2.300	-204.09997	-204.30642
155.0	3.500	2.300	-204.10631	-204.31432
140.0	3.500	2.300	-204.11543	-204.32524
80.0	3.500	2.300	-204.09295	-204.30351
65.0	3.500	2.300	-204.06082	-204.27772
125.0	3.500	2.300	-204.12296	-204.33385
125.0	3.300	2.300	-204.11837	-204.33307
125.0	3.700	2.300	-204.12926	-204.33694
125.0	3.500	2.100	-204.10220	-204.31457
125.0	3.500	2.500	-204.11530	-204.32282
125.0	3.300	2.500	-204.11307	-204.32467
125.0	3.300	2.100	-204.09593	-204.31290
125.0	3.100	2.300	-204.11795	-204.33625
125.0	3.700	2.100	-204.10926	-204.31982
125.0	3.700	2.500	-204.12028	-204.32433

95.0	3.500	2.300	-204.11609	-204.32667
95.0	3.300	2.300	-204.11011	-204.32490
95.0	3.700	2.300	-204.12364	-204.33076
95.0	3.500	2.100	-204.09268	-204.30678
95.0	3.500	2.500	-204.11151	-204.31945
95.0	3.300	2.500	-204.10984	-204.32172
95.0	3.100	2.300	-204.10783	-204.32659
95.0	3.300	2.100	-204.08299	-204.30044
95.0	3.700	2.100	-204.10221	-204.31351
95.0	3.700	2.500	-204.11638	-204.32079

Table AII. Energies for The $N + O_2 \rightarrow NO + O$ Reaction

$^4A'$ Surface

θ	r_{NO}	r_{OO}	E(CASSCF)	E(CCI + Q)
110.0	2.900	2.600	-204.11047	-204.32589
110.0	2.900	2.450	-204.11104	-204.32985
110.0	2.900	2.300	-204.10257	-204.32372
110.0	2.900	2.150	-204.07811	-204.30111
110.0	3.100	2.600	-204.10472	-204.31883
110.0	3.100	2.450	-204.10863	-204.32520
110.0	3.100	2.300	-204.10433	-204.32291
110.0	3.100	2.150	-204.08485	-204.30486
110.0	3.300	2.600	-204.10136	-204.31208
110.0	3.300	2.450	-204.10881	-204.32185
110.0	3.300	2.300	-204.10845	-204.32337
110.0	3.300	2.150	-204.09297	-204.30841
110.0	3.500	2.600	-204.10203	-204.30888
110.0	3.500	2.450	-204.11258	-204.32173
110.0	3.500	2.300	-204.11515	-204.32574
110.0	3.500	2.150	-204.10219	-204.31622
180.0	3.300	2.300	-204.07296	-204.28140
160.0	3.300	2.300	-204.07667	-204.28711
140.0	3.300	2.300	-204.09144	-204.30489
120.0	3.300	2.300	-204.10594	-204.32058
100.0	3.300	2.300	-204.10600	-204.32122
80.0	3.300	2.300	-204.07837	-204.29650
109.4	3.310	2.359	-204.11015	-204.32422

Table AIII. Energies for The O + N_2 → NO + N Reaction

$^3A''$ Surface

θ	r_{NO}	r_{NN}	E(CASSCF)	E(CCI + Q)
110.0	2.400	20.000	-183.78330	-183.93381
110.0	2.300	20.000	-183.79517	-183.94655
110.0	2.200	20.000	-183.80077	-183.95309
110.0	2.100	20.000	-183.79674	-183.95006
110.0	2.000	20.000	-183.77843	-183.93281
90.0	2.175	20.000	-183.80125	
110.0	20.000	20.000	-183.60731	-183.73305
110.0	2.400	4.500	-183.77828	-183.93210
110.0	2.400	4.000	-183.77419	-183.93152
110.0	2.400	3.500	-183.77362	-183.93746
110.0	2.400	3.000	-183.78342	-183.95445
110.0	2.300	4.500	-183.79017	-183.94485
110.0	2.300	4.000	-183.78587	-183.94406
110.0	2.300	3.500	-183.78404	-183.94840
110.0	2.300	3.000	-183.78992	-183.96090
110.0	2.200	5.000	-183.79874	-183.95288
110.0	2.200	4.500	-183.79595	-183.95160
110.0	2.200	4.000	-183.79163	-183.95083
110.0	2.200	3.500	-183.78875	-183.95378
110.0	2.200	3.000	-183.79052	-183.96160
110.0	2.100	4.500	-183.79231	-183.94911
110.0	2.100	4.000	-183.78823	-183.94867
110.0	2.100	3.500	-183.78458	-183.95046
110.0	2.100	3.000	-183.78205	-183.95335
110.0	2.000	4.500	-183.77473	-183.93531
110.0	2.000	4.000	-183.77121	-183.93617
110.0	2.000	3.500	-183.76717	-183.93693

110.0	2.000	3.000	-183.76011	-183.93172
90.0	2.175	4.000	-183.78604	
120.0	2.175	4.000	-183.78992	
150.0	2.175	4.000	-183.77538	
100.0	2.200	4.500	-183.79559	-183.95130
100.0	2.200	4.000	-183.79062	-183.94997
100.0	2.200	3.500	-183.78663	-183.95203
120.0	2.200	4.500	-183.79498	-183.95047
120.0	2.200	4.000	-183.78974	-183.94859
120.0	2.200	3.500	-183.78510	-183.94977
180.0	2.200	4.000	-183.76623	-183.92216
170.0	2.200	4.000	-183.76764	-183.92359
150.0	2.200	4.000	-183.77528	-183.93215
130.0	2.200	4.000	-183.78574	-183.94402
90.0	2.200	4.000	-183.78600	-183.94541
70.0	2.200	4.000	-183.76124	-183.92177
108.9	2.172	4.102	-183.79272	-183.95133
110.0	2.150	4.000	-183.79132	
110.0	2.150	3.750	-183.78931	
110.0	2.200	3.750	-183.78970	
110.0	2.300	3.750	-183.78422	
110.0	2.150	3.500	-183.78802	
110.0	2.200	3.500	-183.78875	
110.0	2.300	3.500	-183.78404	
110.0	2.150	3.250	-183.78764	
110.0	2.200	3.250	-183.78916	
110.0	2.300	3.250	-183.78602	
110.0	2.150	3.000	-183.78766	
110.0	2.200	3.000	-183.70052	
110.0	2.300	3.000	-183.78992	
130.0	3.000	2.200	-183.83306	
110.0	3.500	2.200	-183.87763	

130.0	3.500	2.200	-183.87906	
150.0	3.500	2.200	-183.87666	
130.0	4.000	2.200	-183.90618	
90.0	20.000	2.300	-183.90302	-184.04786
90.0	20.000	2.200	-183.92068	-184.06625
90.0	20.000	2.100	-183.92915	-184.07564
90.0	20.000	2.000	-183.92372	-184.07127
90.0	20.000	1.900	-183.89795	-184.04668

Table AIV. Energies for The $O + N_2 \rightarrow NO + N$ Reaction

$^3A'$ Surface

θ	r_{NO}	r_{NN}	E(CASSCF)	E(CCI + Q)
110.0	2.200	20.000	-183.80109	-183.95330
110.0	2.400	4.500	-183.77369	-183.92704
110.0	2.400	4.000	-183.76149	-183.91802
110.0	2.400	3.500	-183.74421	-183.91249
110.0	2.400	3.000	-183.75507	-183.93458
110.0	2.300	4.500	-183.78542	-183.93945
110.0	2.300	4.000	-183.77280	-183.92984
110.0	2.300	3.500	-183.75354	-183.92247
110.0	2.300	3.000	-183.75889	-183.94088
110.0	2.200	5.000	-183.79692	-183.95067
110.0	2.200	4.500	-183.79093	-183.94573
110.0	2.200	4.000	-183.77797	-183.93569
110.0	2.200	3.500	-183.75715	-183.92707
110.0	2.200	3.000	-183.75776	-183.94186
110.0	2.100	4.500	-183.78686	-183.94253
110.0	2.100	4.000	-183.77366	-183.93223
110.0	2.100	3.500	-183.75174	-183.92322
110.0	2.100	3.000	-183.74858	-183.93369
110.0	2.000	4.500	-183.76860	-183.92524
110.0	2.000	4.000	-183.75530	-183.91493
110.0	2.000	3.500	-183.73289	-183.90679
110.0	2.000	3.000	-183.72711	-183.91248
180.0	2.200	3.500	-183.73027	-183.89056
170.0	2.200	3.500	-183.73211	-183.89314
150.0	2.200	3.500	-183.74202	-183.90772
130.0	2.200	3.500	-183.75360	-183.92309
90.0	2.200	3.500	-183.74054	-183.90841

70.0	2.200	3.500	-183.67801	-183.84481
116.5	2.210	3.574	-183.76030	-183.92696
130.0	3.000	2.200	-183.82618	
130.0	3.500	2.200	-183.87385	
150.0	4.000	2.200	-183.90082	
130.0	4.000	2.200	-183.90161	
110.0	4.000	2.200	-183.90108	
90.0	4.000	2.200	-183.89571	
130.0	5.000	2.200	-183.91812	
90.0	20.000	2.200	-183.92066	